8886 *Inorg. Chem.* **2010**, *49*, 8886–8896
DOI: 10.1021/ic101132z

Inorganic Chemistry
Article

Slow Magnetic Relaxation and Charge-Transfer in Cyano-Bridged Coordination Clusters Incorporating $[Re(CN)_7]^{3-/4-}$

Joseph M. Zadrozny,[†] Danna E. Freedman,[†] David M. Jenkins,[†,‡] T. David Harris,[†] Anthony T. Iavarone,[†,§] Corine Mathonière,[∥] Rodolphe Clérac,[⊥,⊗] and Jeffrey R. Long*[,†]

[†]*Department of Chemistry, University of California, Berkeley, California 94720,* [‡]*Department of Chemistry, University of Tennessee, Knoxville, Tennessee 37996,* [§]*QB3/Chemistry Mass Spectrometry Facility, University of California, Berkeley, California 94720,* [∥]*CNRS, Université de Bordeaux, Institut de Chimie de la Matière Condensée de Bordeaux (ICMCB), 87 avenue du Dr. Albert Schweitzer, Pessac, F-33605 Cedex, France,* [⊥]*CNRS, UPR 8641, Centre de Recherche Paul Pascal (CRPP), Equipe "Matériaux Moléculaires Magnétiques", 115 avenue du Dr. Albert Schweitzer, Pessac, F-33600, France, and* [⊗]*Université de Bordeaux, UPR 8641, Pessac, F-33600, France*

Received June 4, 2010

Treatment of the cyanometalate building unit $[Re(CN)_7]^{3-}$ with $[(PY5Me_2)M(MeCN)]^{2+}$ (M = Co, Ni, Cu) affords a series of pentanuclear clusters of formulas $[(PY5Me_2)_4M_4Re(CN)_7]^{5+}$ (M = Co, Ni, Cu) and $[(PY5Me_2)_4Cu_4Re(CN)_7]^{4+}$. Single crystal X-ray diffraction analyses of the clusters reveal a star-like structure in which four $[(PY5Me_2)M]^{2+}$ moieties are linked to a central $[Re(CN)_7]^{3-}$ unit via bridging cyanide ligands. An intramolecular $Co^{II} \rightarrow Re^{IV}$ charge-transfer accompanies the formation of the $Co^{II}_4Re^{IV}$ cluster, giving a $Co^{II}_3Co^{III}Re^{III}$ species. Spectroelectrochemical methods and irradiation experiments are used to characterize the metal−metal charge-transfer bands of this compound. A rhenium-based thermally induced one-electron reduction is observed for the $Cu^{II}_4Re^{IV}$ cluster to give a $Cu^{II}_4Re^{III}$ complex; however, this reduction may be forestalled at low temperature. Finally, magnetic measurements reveal intracluster ferromagnetic exchange coupling, strong uniaxial magnetic anisotropy, and slow magnetic relaxation in the $Ni^{II}_4Re^{IV}$ and $Cu^{II}_4Re^{IV}$ clusters.

Introduction

In the early 1990s, the molecular cluster $Mn_{12}O_{12}(O_2CCH_3)_{16}(H_2O)_4$ was shown to display slow magnetic relaxation at low temperatures, similar to the behavior of a superparamagnet below its blocking temperature.[1] Molecules of this type, referred to as single-molecule magnets, exhibit slow relaxation because of an energy barrier to magnetization reversal created by action of a negative axial zero-field splitting, D, on the spin ground state, S (according to the Hamiltonian $H = DS_z^2$, where S_z is the component of S along the z direction). This energy barrier can be expressed as $U = S^2|D|$ for integer values of S or $U = (S^2 - {}^1/_4)|D|$ for half-integer values of S. Ultimately, the magnetic bistability of single-molecule magnets could find use in potential applications such as high-density information storage or quantum computing.[2]

One method for synthesizing new single-molecule magnets centers on the use of a building-block approach to target high-nuclearity clusters where the metal ions are linked by cyanide bridging ligands.[3,4] This method exploits the predictable coordination chemistry of the cyanide ion, where one cyanide ligand is expected to bridge only two metals in an approximate linear geometry. Typical cluster preparation involves two building units, where one unit features one or more terminal cyanide ligands and the other unit bears one or more coordination sites occupied by labile solvent molecules. In solution, the nucleophilic nitrogen ends of the terminal

*To whom correspondence should be addressed. E-mail: jrlong@berkeley.edu.

(1) (a) Lis, T. *Acta Crystallogr., Sect. B* **1980**, *36*, 2042. (b) Sessoli, R.; Gatteschi, D.; Caneschi, A.; Novak, M. A. *Nature* **1993**, *365*, 141. (c) Sessoli, R. T.; Hui, L.; Schake, A. R.; Wang, S.; Vincent, J. B.; Folting, K.; Gatteschi, D.; Christou, G.; Hendrickson, D. N. *J. Am. Chem. Soc.* **1993**, *115*, 1804.

(2) (a) Garanin, D. A.; Chudnovsky, E. M. *Phys. Rev. B* **1997**, *56*, 11102. (b) Leuenberger, M. N.; Loss, D. *Nature* **2001**, *410*, 789. (c) Jo, M.-H.; Grose, J. E.; Liang, W.; Baheti, K.; Deshmukh, M. M.; Sokol, J. J.; Rumberger, E. M.; Hendrickson, D. N.; Long, J. R.; Park, H.; Ralph, D. C. *Nano Lett.* **2006**, *6*, 2014. (d) Ardavan, A.; Rival, O.; Morton, J. J. L.; Blundell, S. J.; Tyryshkin, A. M.; Timco, G. A.; Winpenny, R. E. P. *Phys. Rev. Lett.* **2007**, *98*, 057201. (e) Bogani, L.; Wernsdorfer, W. *Nat. Mater.* **2008**, *7*, 884. (f) Stamp, P. C. E.; Gaita-Arino, A. *J. Mater. Chem.* **2009**, *19*, 1718.

(3) (a) Long, J. R. Molecular Cluster Magnets. In *Chemistry of Nanostructured Materials*; Yang, P., Ed.; World Scientific: Hong Kong, 2003; pp 291−315 and references therein. (b) Beltran, L. M. C.; Long, J. R. *Acc. Chem. Res.* **2005**, *38*, 325. (c) Shatruk, M.; Avendano, C.; Dunbar, K. In *Progress in Inorganic Chemistry*; Karlin, K. D., Ed.; John Wiley & Sons: Amsterdam, 2009, Vol. *56*, p 155 and references therein.

 Published on Web 08/30/2010

cyanide ligands displace these solvent molecules, thereby leading to a multinuclear assembly. By judicious selection of polydentate capping ligands for either of the two building units, one can direct the formation of a variety of molecular structures. In addition to this structural control, qualitative rules for predicting the nature of the magnetic superexchange coupling between two cyano-bridged metal centers are well established via exhaustive studies on Prussian Blue analogues.[5] This combination of structural and magnetic predictability has led to the rational design of a wide variety of cyano-bridged magnetic molecules.[3,4]

In 2003, the homoleptic cyanometalate complex $[Re(CN)_7]^{3-}$ was prepared and shown to exhibit strong magnetic anisotropy.[6] This anisotropy can be attributed to a combination of the unquenched orbital angular momentum afforded by the $^2E_1''$ electronic ground state and the large spin−orbit coupling associated with the heavy rhenium atom.[7] We thus hypothesized that incorporating $[Re(CN)_7]^{3-}$ into a high-spin cluster would impart magnetic anisotropy to the assembly, thereby leading to slow magnetic relaxation. Indeed, the pentanuclear cyano-bridged cluster $[(PY5Me_2)_4Mn_4Re(CN)_7]^{5+}$ ($PY5Me_2$ = 2,6-bis(1,1-bis(2-pyridyl)ethyl)pyridine)) was prepared and shown to exhibit the highest relaxation barrier (U_{eff} = 33 cm^{-1}) yet observed for a cyano-bridged single-molecule magnet.[8] One considerable drawback to the preparation of this cluster, however, is that it requires low-temperature conditions, as the 4+ oxidation state of the rhenium ion becomes destabilized upon cluster formation. Indeed, upon warming to room temperature, the paramagnetic Re^{IV} ion undergoes a spontaneous, solvent-assisted, one-electron reduction to the diamagnetic Re^{III} ion. This thermal instability has precluded significant study of the Mn_4Re cluster, owing to preparative and handling difficulties.

Electrochemical investigations of Prussian Blue analogues have shown that the reduction potential of ferricyanide is shifted toward a more positive potential as other metals are appended to it, a consequence of polarization effects by M′.[9] Furthermore, these studies have revealed that this general effect becomes more pronounced as the charge/radius ratio of the M′ ion increases. In view of this trend, we sought to substitute more electron-rich metal ions (Co^{II}, Ni^{II}, Cu^{II}) in place of Mn^{II} in the synthesis of clusters of formulas $[(PY5Me_2)_4M_4Re(CN)_7]^{5+}$ with the expectation that such a substitution would stabilize the Re^{IV} ion toward reduction.

The selection of Co^{II}, Ni^{II}, and Cu^{II} for incorporation into the M_4Re clusters was not driven simply by their electron density relative to Mn^{II}. For instance, the unquenched orbital angular momentum present in octahedrally coordinated Co^{II} ion should enhance the anisotropy of the overall cluster. Furthermore, the unpaired electron of Re^{IV} in $[Re(CN)_7]^{3-}$ lies in an orbital of π-type symmetry.[7] Exchange coupling with high-spin Mn^{II} is therefore expected to be weak because of competing ferromagnetic and antiferromagnetic contributions from electrons residing in d_σ and d_π-type orbitals of the Mn^{II} ion.[10] Indeed, fits to the magnetic susceptibility data obtained for the Mn_4Re cluster reveal a coupling constant of only J = 2.3 cm^{-1}. In contrast, the octahedral coordination geometry of a $[(PY5Me_2)M(NC)]^{2+}$ fragment should promote strictly ferromagnetic Re···M exchange for Ni^{II} and Cu^{II} ions, which both bear unpaired electrons in only σ-type orbitals. In fact, a recent report has demonstrated very strong ferromagnetic coupling between Re^{IV} and Cu^{II} ions through a cyanide ligand.[11] Herein, we report the syntheses of the building units $[(PY5Me_2)M(MeCN)](PF_6)_2$ (M = Co (**4**), Ni (**5**), Cu (**6**)) and their subsequent incorporation into the cyano-bridged cluster compounds $[(PY5Me_2)_4M_4Re(CN)_7](PF_6)_5$ (M = Co (**7**), Ni (**8**), Cu (**10**)), and $[(PY5Me_2)_4Cu_4Re(CN)_7](PF_6)_4$ (**9**). Notably, the use of **5** enables preparation of the Ni_4Re cluster, where the Re^{IV} ion is stable toward reduction. In contrast, **10** is thermally unstable, and preparation at room temperature triggers a reduction of the Re^{IV} ion. Moreover, slow magnetic relaxation is observed for clusters **8** and **10**, where the Re ion remains in the 4+ oxidation state. Finally, an intramolecular charge-transfer occurs during the synthesis of **7**, yielding a $Co^{II}{}_3Co^{III}Re^{III}$ cluster.

Experimental Section

Preparation of Compounds. Unless otherwise noted, all procedures were performed under an inert N_2 atmosphere using standard glovebox techniques. The ligand 2,6-bis(1,1-bis(2-pyridyl)ethyl)pyridine ($PY5Me_2$)[12] and the compound $(Bu_4N)_3[Re(CN)_7]$[6] were synthesized as previously described. Acetonitrile (MeCN), diethylether (Et_2O), and tetrahydrofuran (THF) were dried by circulation over alumina for 16 h prior to use, and were then deoxygenated by sparging with N_2 for at least 1 h. Propionitrile (EtCN) and diisopropylether (*i*-Pr_2O) were

(4) Selected References: (a) Mallah, T.; Auberger, C.; Verdaguer, M.; Veillet, P. *Chem. Commun.* **1995**, 61. (b) Parker, R. J.; Hockless, D. C. R.; Moubaraki, B.; Murray, K. S.; Spiccia, L. *Chem. Commun.* **1996**, 2789. (c) Zhong, Z. J.; Seino, H.; Mizobe, Y.; Hidai, M.; Fujishima, A.; Ohkoshi, S.-I.; Hashimoto, K. *J. Am. Chem. Soc.* **2000**, *122*, 2952. (d) Berlinguette, C. P.; Vaughn, D.; Cañada-Vilalta, C.; Galán-Mascarós, J. R.; Dunbar, K. R. *Angew. Chem., Int. Ed.* **2003**, *42*, 1523. (e) Marvaud, V.; Decroix, C.; Scuiller, A.; Guyard-Duhayon, C.; Vaissermann, J.; Gonnet, F.; Verdaguer, M. *Chem.—Eur. J.* **2003**, *9*, 1677. (f) Schelter, E. J.; Prosvirin, A. V.; Dunbar, K. R. *J. Am. Chem. Soc.* **2004**, *126*, 15004. (g) Wang, S.; Zou, J.-L.; Zhou, H.-C.; Choi, H. J.; Ke, Y.; Long, J. R.; You, X.-Z. *Angew. Chem., Int. Ed.* **2004**, *43*, 5940. (h) Song, Y.; Zhang, P.; Ren, X.-M.; Shen, X.-F.; Li, Y.-Z.; You, X.-Z. *J. Am. Chem. Soc.* **2005**, *127*, 3708. (i) Li, D.; Parkin, S.; Wang, G.; Yee, G. T.; Prosvirin, A. V.; Holmes, S. M. *Inorg. Chem.* **2005**, *44*, 4903. (j) Ni, Z.-H.; Kou, H.-Z.; Zhang, L.-F.; Ge, C.; Cui, A.-L.; Wang, R.-J.; Li, Y.; Sato, O. *Angew. Chem., Int. Ed.* **2005**, *44*, 7742. (k) Wang, C.-F.; Zuo, J.-L.; Bartlett, B. M.; Song, Y.; Long, J. R.; You, X.-Z. *J. Am. Chem. Soc.* **2006**, *128*, 7162. (l) Li, D.; Parkin, S.; Wang, G.; Yee, G. T.; Clérac, R.; Wernsdorfer, W.; Holmes, S. M. *J. Am. Chem. Soc.* **2006**, *128*, 4214. (m) Glaser, T.; Heidemeier, M.; Weyhermüller, T.; Hoffmann, R.-D.; Rupp, H.; Müller, P. *Angew. Chem., Int. Ed.* **2006**, *45*, 6033. (n) Lim, J. H.; Yoon, J. H.; Kim, H. C.; Hong, C. S. *Angew. Chem., Int. Ed.* **2006**, *45*, 7424. (o) Harris, T. D.; Long, J. R. *Chem. Commun.* **2007**, 1360. (p) Shatruk, M.; Dragulescu Andrasi, A.; Chambers, K. E.; Stoian, S. A.; Bominaar, E. L.; Achim, C.; Dunbar, K. R. *J. Am. Chem. Soc.* **2007**, *129*, 6104.

(5) (a) Weihe, H.; Güdel, H. *Comments Inorg. Chem.* **2000**, *22*, 75. (b) Ruiz, E.; Rodríguez-Fortea, A.; Alvarez, S.; Verdaguer, M. *Chem.—Eur. J.* **2005**, *11*, 2135. (c) Atanasov, M.; Comba, P.; Daul, C. *J. Phys. Chem. A* **2006**, *110*, 13332. (d) Rebilly, J.-N.; Mallah, T. Synthesis of Single−Molecule Magnets Using Metallocyanates. In *Single−Molecule Magnets and Related Phenomena*; Winpenny, R., Ed.; Springer: Berlin, 2006; pp 103−131.

(6) Bennett, M. V.; Long, J. R. *J. Am. Chem. Soc.* **2003**, *125*, 2394.

(7) Jorge, D.; Mendizabal, F.; Ramiro, A.-P. *J. Phys. Chem. A* **2006**, *110*, 1072.

(8) Freedman, D. E.; Jenkins, D. M.; Iavarone, A. T.; Long, J. R. *J. Am. Chem. Soc.* **2008**, *130*, 2884.

(9) Scholz, F.; Dostal, A. *Angew. Chem., Int. Ed. Engl.* **1996**, *34*, 2685.

(10) (a) Carlin, R. L. *Magnetochemistry*; Springer-Verlag: Berlin Heidelberg, 1986. (b) Kahn, O. *Molecular Magnetism*; John Wiley & Sons: New York, 1993. (c) Figgis, B. N.; Hitchman, M. A. *Ligand Field Theory and Its Applications*; Wiley-VCH: New York, 2000. (d) Lloret, F.; Julve, M.; Cano, J.; Ruiz-García, R.; Pardo, E. *Inorg. Chim. Acta* **2008**, *361*, 3432.

(11) Harris, T. D.; Coulon, C.; Clérac, R.; Long, J. R., submitted for publication.

(12) Bechlars, B.; D'Alessandro, D. M.; Jenkins, D. M.; Iavarone, A. T.; Glover, S. D.; Kubiak, C. P.; Long, J. R. *Nat. Chem.* **2010**, *2*, 362.

distilled over CaH_2 and degassed prior to use. Diatomaceous earth (Celite 545) was purchased from Fisher Scientific and dried by heating under vacuum. All other reagents were obtained from commercial vendors and used without further purification.

[(PY5Me$_2$)CoI]I (1). Solid $PY5Me_2$ (1.0 g, 2.3 mmol) and CoI_2 (0.72 g, 2.3 mmol) were added to 100 mL of THF and stirred for 48 h, giving a yellow solid. The precipitate was collected on a fine fritted glass filter, washed with successive aliquots of THF (2 × 30 mL) and Et_2O (2 × 30 mL), and dried in vacuo for 2 h to give 1.6 g (96%) of product. IR (neat): 1594(s), 1477(m), 1464(s), 1450(m), 1435(s), 1294(m), 1253(w), 1230(w), 1201(w), 1066(w), 1078(w), 1061(m), 1015(m), 865(m), 792(m), 751(s) cm^{-1}. ESI-MS (*m*/*z*): $\{[(PY5Me_2)CoI]\}^+$, 629.1. UV−vis (MeCN): λ_{max} (ε_M, M^{-1} cm^{-1}) 366 (110), 500 (9), 900 (11) nm. Anal. Calcd. for $C_{29}H_{25}CoI_2N_5$: C, 46.05; H, 3.33; N, 9.26%. Found: C, 45.89; H, 3.54; N, 9.65%.

[(PY5Me$_2$)NiI]I (2). Solid $PY5Me_2$ (1.1 g, 2.4 mmol) and NiI_2 (0.77 g, 2.5 mmol) were added to 100 mL of THF and stirred for 48 h, giving a gray solid. The precipitate was collected on a fine fritted glass filter, washed with successive aliquots of THF (2 × 30 mL) and Et_2O (2 × 30 mL), and dried in vacuo for 2 h to give 1.5 g (83%) of product. IR (neat): 1595(s), 1478(m), 1464(s), 1452(m), 1437(s), 1386(m), 1295(m), 1166(w), 1063(m), 1017(m), 863(m), 791(m), 766(m), 752(s) cm^{-1}. ESI-MS (*m*/*z*): $\{[(PY5Me_2)Ni]\}^{2+}$, 251.0; $\{[(PY5Me_2)NiI]\}^+$, 628.0. UV−vis (MeCN): λ_{max} (ε_M, M^{-1} cm^{-1}) 320 (1197), 430 (37), 524 (18), 802 (17), 877 (15) nm. Anal. Calcd. for $C_{29}H_{25}I_2N_5Ni$: C, 46.07; H, 3.33; N, 9.27%. Found: C, 46.38; H, 3.51; N, 8.93%.

[(PY5Me$_2$)CuCl]Cl (3). Solid $CuCl_2$ (0.15 g, 1.1 mmol) and $PY5Me_2$ (0.49 g, 1.1 mmol) were added to 20 mL of THF and stirred for 48 h, giving a blue solid. The precipitate was collected on a fine fritted glass filter, washed with successive aliquots of THF (2 × 30 mL) and Et_2O (2 × 30 mL), and dried in vacuo for 2 h to give 0.59 g (93%) of product. IR (neat): 1598(s), 1588(s), 1580(s), 1471(s), 1463(s), 1456(s), 1438(s), 1424(s), 1370(m), 1296(m), 1223(w), 1202(w), 1173(m), 1153(m), 1104(m), 1068(m), 1057(m), 1029(m), 1011(m), 993(m), 869(m), 842(m), 779(s), 755(s), 749(s), 655(m) cm^{-1}. ESI-MS (*m*/*z*): $\{[(PY5Me_2)CuCl]\}^+$, 541; $\{[(PY5Me_2)Cu]\}^{2+}$, 253. UV−vis (MeCN): λ_{max} (ε_M, M^{-1} cm^{-1}) 468 (18), 616 (74), 950 (11) nm. Anal. Calcd. for $C_{29}H_{25}Cl_2CuN_5$: C, 60.26; H, 4.36; N, 12.12%. Found: C, 59.92; H, 4.54; N, 11.83%.

[(PY5Me$_2$)Co(MeCN)](PF$_6$)$_2$ (4). Solid $TlPF_6$ (0.29 g, 0.83 mmol) was added to a solution containing **1** (0.29 g, 0.39 mmol) in 9 mL of MeCN, resulting in an orange solution and a yellow precipitate. After stirring for 48 h, the orange mixture was filtered through diatomaceous earth to remove the yellow solid. Vapor diffusion of Et_2O into the orange filtrate gave 0.22 g (69%) of product as orange, block-shaped crystals suitable for X-ray analysis. IR (neat): 2302(m), 2275(m), 1599(s), 1591(s), 1484(m), 1470(s), 1457(m), 1441(m), 1110(w), 1063(m), 1022(m), 828(vs), 758(s), 635(m) cm^{-1}. ESI-MS (*m*/*z*): $\{[(PY5Me_2)Co]\}^{2+}$, 249.1; $\{[(PY5Me_2)Co](PF_6)\}^+$, 643.1; $\{[(PY5Me_2)Co(MeCN)](PF_6)\}^+$, 685.1. UV−vis (MeCN): λ_{max} (ε_M, M^{-1} cm^{-1}) 257 (43100), 308 (sh) (4300), 450 (48) nm. Anal. Calcd. for $C_{31}H_{28}CoF_{12}N_6P_2$: C, 44.67; H, 3.39 ; N, 10.09%. Found: C, 44.52; H, 3.36; N, 10.02%.

[(PY5Me$_2$)Ni(MeCN)](PF$_6$)$_2$ (5). Solid $TlPF_6$ (0.38 g, 1.1 mmol) was added to a solution containing **2** (0.40 g, 0.53 mmol) in 14 mL of MeCN, resulting in an orange solution and yellow precipitate. After stirring for 48 h, the orange mixture was filtered through diatomaceous earth to remove the yellow solid. Vapor diffusion of Et_2O into the orange filtrate gave 0.30 g (65%) of product as pink, block-shaped crystals suitable for X-ray analysis. IR (neat): 2273(w), 1596(s), 1484(m), 1469(s), 1457(m), 1441(m), 1064(m), 1021(m), 881(m), 827(vs), 795(m), 757(s), 652(m), 629(m) cm^{-1}. ESI-MS (*m*/*z*): $\{[(PY5Me_2)Ni]\}^{2+}$, 250.6. UV−vis (MeCN): λ_{max} (ε_M, M^{-1} cm^{-1}) 307 (1350), 432 (4), 529 (8), 863 (17), 794 (18) nm. Anal. Calcd. for $C_{31}H_{28}F_{12}N_6NiP_2$: C, 44.69; H, 3.39; N, 10.09%. Found: C, 44.38; H, 3.24; N, 10.13%.

[(PY5Me$_2$)Cu(MeCN)](PF$_6$)$_2$ (6). Solid $TlPF_6$ (0.27 g, 0.77 mmol) was added to a solution containing **3** (0.21 g, 0.36 mmol) in 16 mL of MeCN, resulting in a blue solution and a white precipitate. After stirring for 48 h, the blue mixture was filtered through diatomaceous earth to remove the white solid. Vapor diffusion of Et_2O into the blue filtrate gave 0.22 g (70%) of product as blue, block-shaped crystals suitable for X-ray analysis. IR (neat): 2312(w), 2284(w), 1596(s), 1586(s), 1468(s), 1456(s), 1441(m), 1398(m), 1303(w), 1064(m), 1018(m), 828(vs), 792(m), 775(m), 758(s) cm^{-1}. ESI-MS (*m*/*z*): $\{[(PY5Me_2)Cu](PF_6)\}^+$, 652; $\{[(PY5Me_2)Cu]\}^{2+}$, 254. UV−vis (MeCN): λ_{max} (ε_M, M^{-1} cm^{-1}) 605 (75), 928 (13) nm. Anal. Calcd. for $C_{31}H_{28}CuF_{12}N_6P_2$: C, 44.43; H, 3.37; N, 10.03%. Found: C, 44.26; H, 3.30; N, 9.89%.

[(PY5Me$_2$)$_4$Co$_4$Re(CN)$_7$](PF$_6$)$_5$ (7). A solution containing $(Bu_4N)_3[Re(CN)_7]$ (21 mg, 0.019 mmol) in 3 mL of MeCN was added to a solution containing **4** (63 mg, 0.075 mmol) in 3 mL of MeCN to give a purple solution. Vapor diffusion of Et_2O into this solution afforded 45 mg (77%) of product as red, plate-shaped crystals suitable for X-ray analysis. IR (neat): 2102(s), 2056(s), 1640(w), 1594(s), 1480(w), 1467(s), 1440(m), 1393(m), 1253(w), 1170(w), 1058(w), 1019(w), 830(vs), 757(s) cm^{-1}. ESI-MS (*m*/*z*): $\{[(PY5Me_2)_4Co_4Re(CN)_7](PF_6)_3\}^{2+}$, 1406; $\{[(PY5Me_2)_3Co_3Re(CN)_7]\}^{3+}$, 625 (base peak); $\{[(PY5Me_2)_3Co_3Re(CN)_7](PF_6)\}^{2+}$, 1009.5; $\{[(PY5Me_2)_3Co_3Re(CN)_7](PF_6)_2\}^+$, 2164; $\{[(PY5Me_2)_3Co_3Re(CN)_7]\}^{2+}$, 937; $\{[(PY5Me_2)_2Co_2Re(CN)_7]\}^+$, 1372; $\{[(PY5Me_2)_2Co_2Re(CN)_7]\}^{2+}$, 686; $\{[(PY5Me_2)_2Co_2Re(CN)_7](PF_6)\}^+$, 1517. UV−vis (MeCN): λ_{max} (ε_M, M^{-1} cm^{-1}) 510 (1680), 854 (1600) nm. Anal. Calcd. for $C_{123}H_{100}Co_4F_{30}N_{27}P_5Re$: C, 47.61; H, 3.25; N, 12.19%. Found: C, 47.27; H, 3.36; N, 12.49%.

[(PY5Me$_2$)$_4$Ni$_4$Re(CN)$_7$](PF$_6$)$_5$ (8). A solution containing $(Bu_4N)_3[Re(CN)_7]$ (16 mg, 0.015 mmol) in 1 mL of MeCN was added to a solution containing **5** (50 mg, 0.06 mmol) in 2 mL of MeCN to give a dark yellow-brown solution. Vapor diffusion of Et_2O into this solution afforded 18 mg (40%) of product as dark yellow, needle-shaped crystals suitable for X-ray analysis. IR (neat): 2120(w), 2089(w), 1596(s), 1480(m), 1468(m), 1454(m), 1441(m), 1390(w), 1169(w), 1111(w), 1062(m), 1021(m), 834(s), 792(m), 757(s) cm^{-1}. ESI-MS (*m*/*z*): $\{[(PY5Me_2)_4Ni_4Re(CN)_7](PF_6)_3\}^{2+}$, 1406; $\{[(PY5Me_2)_4Ni_4Re(CN)_7](PF_6)_2\}^{3+}$, 888; $\{[(PY5Me_2)_3Ni_3Re(CN)_7](PF_6)\}^{2+}$, 1008; $\{[(PY5Me_2)_3Ni_3Re(CN)_7]\}^{3+}$, 623 (base peak). Anal. Calcd. for $C_{123}H_{100}F_{30}N_{27}Ni_4P_5Re$: C, 47.62; H, 3.24; N, 12.19%. Found; C, 47.39; H, 3.56; N, 12.11%.

[(PY5Me$_2$)$_4$Cu$_4$Re(CN)$_7$](PF$_6$)$_4$ (9). A solution containing $(Bu_4N)_3[Re(CN)_7]$ (17 mg, 0.016 mmol) in 1 mL of EtCN was added to a solution containing **6** (53 mg, 0.063 mmol) in 3 mL of EtCN to give a dark blue solution, which was stirred for 48 h. Vapor diffusion of *i*-Pr_2O into this solution produced 40 mg (87%) of product as dark blue, plate-shaped crystals suitable for X-ray analysis. IR (neat): 2287(w), 2256(w), 1587(m), 1467(m), 1456(m), 1441(m), 1397(w), 1303(w), 1202(w), 1172(w), 1092(w), 1062(w), 1018(w), 993(w), 907(w), 832(s), 788(m), 773(m), 758(m), 655(m), 632(m), 618(m), 606(m), 581(m), 572(m), 556(s), 538(w) cm^{-1}. ESI-MS (*m*/*z*): $\{[(PY5Me_2)_4Cu_4Re(CN)_7](PF_6)_2\}^{2+}$, 1343; $\{[(PY5Me_2)_4Cu_4Re(CN)_7](PF_6)\}^{3+}$, 847; $\{[(PY5Me_2)_4Cu_4Re(CN)_7]\}^{4+}$, 599; $\{[(PY5Me_2)_3Cu_3Re(CN)_7](PF_6)]\}^{2+}$, 1017; $\{[(PY5Me_2)_3Cu_3Re(CN)_7]\}^{3+}$, 630. Anal. Calcd. for $C_{123}H_{100}Cu_4F_{24}N_{27}P_4Re\cdot EtCN$: C, 48.73; H, 3.33; N, 12.47%. Found: C, 48.48; H, 3.10; N, 12.14%.

[(PY5Me$_2$)$_4$Cu$_4$Re(CN)$_7$](PF$_6$)$_5$ (10). A solution containing $(Bu_4N)_3[Re(CN)_7]$ (21 mg, 0.019 mmol) in 1 mL of MeCN and a solution containing **6** (63 mg, 0.075 mmol) in 2 mL of MeCN were chilled to −42 °C. The solution containing $(Bu_4N)_3[Re(CN)_7]$ was then added dropwise to the other stirred solution to

Table 1. Crystallographic Data[a] for $[(PY5Me_2)M(MeCN)](PF_6)_2$, where M = Co (**4**), Ni (**5**), and Cu (**6**), $[(PY5Me_2)_4M_4Re(CN)_7](PF_6)_5$, where M = Co (**7**) and Ni (**8**), and $[(PY5Me_2)_4Cu_4Re(CN)_7](PF_6)_4$ (**9**)

	4	**5**	**6**	**7**	**8**	**9**
formula	$C_{72}H_{75}Co_2F_{24}N_{15}OP_4$	$C_{72}H_{75}F_{24}N_{15}Ni_2OP_4$	$C_{62}H_{56}Cu_2F_{24}N_{13}P_4$	$C_{133}H_{100}Co_4F_{30}N_{27}P_5Re$	$C_{133}H_{100}F_{30}N_{30}Ni_4OP_5Re$	$C_{123}H_{100}Cu_4F_{24}N_{27}P_4Re$
fw	1864.19	1863.7	1712.17	3103.07	3299.37	2976.54
T, K	140	140	159	150	100	141
space group	$P2_1/c$	$P2_1/c$	$P1$	$C2/c$	$P\bar{1}$	$P\bar{1}$
Z	4	4	2	8	2	2
a, Å	22.419(2)	22.369(5)	11.407(1)	44.679(10)	12.029(1)	18.766(1)
b, Å	15.249(1)	15.229(3)	12.756(1)	18.870(4)	19.932(1)	19.334(1)
c, Å	24.564(2)	24.469(5)	13.182(1)	41.036(9)	32.048(1)	22.556(1)
α, deg	90	90	68.789(1)	90	80.202(3)	113.098(1)
β, deg	107.777(2)	107.777(2)	70.060(1)	107.277(3)	89.201(3)	97.219(1)
γ, deg	90	90	89.688(1)	90	73.901(3)	110.376(1)
V, Å^3	7997(1)	7946(3)	1665.7(2)	33036(13)	7267.2(6)	6722.5(6)
d_{calc}, g/cm^3	1.516	1.396	1.671	1.148	1.466	1.542
R_1 (wR_2), %[b]	5.74 (13.90)	5.72 (14.31)	3.53 (8.16)	10.22 (26.07)	6.28 (14.61)	8.15 (11.43)

[a] Obtained with graphite-monochromated Mo Kα (λ = 0.71073 Å) radiation for **4**, **5**, **6**, **7**, and **9**. Data for **8** were collected with graphite-monochromated Cu Kα (λ = 1.5405 Å) radiation. [b] $R_1 = \sum||F_o| - |F_c||/\sum|F_o|$, $wR_2 = \{\sum[w(F_o^2 - F_c^2)^2]/\sum[w(F_o^2)^2]\}^{1/2}$.

give a dark green solution. The solvent was removed in vacuo to afford the product as an impure dark green solid mixed with $(Bu_4N)PF_6$. All analyses were performed on this mixture. IR (neat): ν_{CN} = 2294(w), 2252(w), 2163(w), 2126(w), 2066(w) cm^{-1}. ESI-MS (m/z): $\{[(PY5Me_2)_4Cu_4Re(CN)_7](PF_6)_3\}^{2+}$, 1415.5; $\{[(PY5Me_2)_4Cu_4Re(CN)_7](PF_6)_2\}^{2+}$, 1343; $\{[(PY5Me_2)_4Cu_4Re(CN)_7](PF_6)\}^{3+}$, 847; $\{[(PY5Me_2)_4Cu_4Re(CN)_7]\}^{4+}$, 599; $\{[(PY5Me_2)_3Cu_3Re(CN)_7](PF_6)\}^{2+}$, 1017; $\{[(PY5Me_2)_3Cu_3Re(CN)_7]\}^{3+}$, 630; $\{[(PY5Me_2)_3Cu_3Re(CN)_7]\}^{2+}$, 944. Anal. Calcd. For $C_{123}H_{100}Cu_4F_{30}N_{27}P_5Re\cdot 3(Bu_4N)PF_6$: C,47.94; H, 4.89; N, 9.81%. Found: C, 47.65; H, 4.85; N, 9.89%.

X-ray Structure Determinations. Structures were determined for compounds **4**, **5**, **6**, **7**, **8**, and **9** (Table 1). X-ray diffraction analyses were performed on single crystals coated with Paratone-N oil and mounted on Kaptan loops. The crystals were frozen under a stream of N_2 during measurements. Data were collected using either a Bruker X8 APEX diffractometer equipped with a Bruker MICROSTAR X-ray source, APEX-II detector, and a Cu anode (λ = 1.5406 Å) (**8**) or a Bruker SMART diffractometer equipped with an APEX detector using MoKα (λ = 0.71073 Å) radiation (**4**, **5**, **6**, **7**, **9**). Raw data were integrated and corrected for Lorentz and polarization effects using Bruker APEX2 v. 2009.1.[13] Absorption corrections were applied using SADABS.[14] Space group assignments were determined by examination of systematic absences, E-statistics, and successive refinement of the structures. Crystal structures were solved by either direct methods (**4**, **5**, **6**, **8**, **9**) or Patterson techniques (**7**) with the aid of successive difference Fourier maps in SHELXL.[15] None of the crystals showed significant decay during data collection. Thermal parameters were refined anisotropically for all non-hydrogen atoms in the main body and PF_6^- counterions of **4**, **5**, **6**, **8**, and **9**. The quality of the collected data for **7** was not sufficient to justify an anisotropic refinement of the thermal parameters for all atoms, and as such anisotropic refinement was restricted to the metal, phosphorus, and fluorine atoms with full occupancy. Hydrogen atoms were placed in ideal positions and refined using a riding model for all structures. Heavy disorder of PF_6^- anions and solvents of crystallization were modeled with the use of free variables. Solvent disorder was extensive and in some cases impossible to model for the structures of **7**, **8**, and **9**. We note that attempts to model the disorder did not significantly alter the metrics for the clusters. For these structures, SQUEEZE[16] was used to account for the unassigned electron density. Additional discussions of structure solutions can be found in the Supporting Information.

Magnetic and Photomagnetic Measurements. Magnetic data were collected using a Quantum Design MPMS-XL or PPMS magnetometer. Measurements for **4**−**9** were obtained on finely ground microcrystalline powders restrained in a frozen eicosane matrix within polycarbonate capsules. Direct current (dc) magnetic susceptibility data were collected in the temperature range 2−300 K under an applied field of 1000 Oe. Alternating current (ac) susceptibility data were collected under zero applied dc field using a 4 Oe ac field oscillating at frequencies from 10 to 1488 Hz. Dc magnetization data were collected in the temperature range 1.8−10 K at fields from 1 to 15 T (**8**) or from 1 to 7 T (**10**). All data were corrected for diamagnetic contributions from the sample holder and eicosane, as well as for core diamagnetism (estimated using Pascal's constants).

A chilled sample of the reaction mixture containing **10** was isolated for measurement in vacuo and restrained in a frozen Et_2O matrix. Because of its thermal instability, the sample could not be completely separated from the diamagnetic side product $(Bu_4N)PF_6$. During the course of the measurements, the sample cavity of the magnetometer was not heated above 230 K to maintain the highest concentration of **10** and to limit the amount of **9** formed as an impurity.

Photomagnetic experiments were performed with a 150 W halogen lamp (LEICA CLS 150X) and different LED sources coupled through an optical fiber directed into the SQUID magnetometer cavity. Powdered samples (2 to 3 mg) were packed in a thermoformed plastic straw maintained at about 3−4 mm from the optical fiber. Data acquired in the absence of light were systematically subtracted from the data acquired after irradiation. This difference was added to dc measurements performed with a standard SQUID setup to get final post-irradiation data.

Electrochemical and Spectroelectrochemical Measurements. Cyclic voltammograms were obtained with a Bioanalytical systems CV-50W voltammograph, a platinum wire counter electrode, a silver wire reference electrode, and a platinum working electrode. Analyte solutions were prepared with 0.1 M solutions of $(Bu_4N)PF_6$ in MeCN. Ferrocene was used as an internal standard and all potentials reported here are referenced to the $Cp_2Fe/[Cp_2Fe]^+$ couple. UV−vis−NIR spectroelectrochemistry over the range of 5000−30,000 cm^{-1} was performed using a CARY

(13) *APEX2*, v. 2009; Bruker Analytical X−Ray Systems, Inc: Madison, WI, 2009.
(14) Sheldrick, G. M. *SADABS*, Version 2.03; Bruker Analytical X−Ray Systems, Inc: Madison, WI, 2000.
(15) Sheldrick, G. M. *SHELXTL*, Version 6.12; Bruker Analytical X−Ray Systems, Inc: Madison, WI, 2000.
(16) Van der Sluis, P.; Spek, A. L. *Acta Crystallogr., Sect. A* **1990**, *46*, 194–201.

5000 spectrophotometer interfaced to Varian WinUV software. The absorption spectra of the electrogenerated species were obtained in situ by the use of an Optically Semi-Transparent Thin-Layer Electrosynthetic (OSTLE) cell, of path length 1.0 mm, mounted in the path of the spectrophotometer. Solutions for the spectroelectrochemical experiment contained 0.1 M $(Bu_4N)PF_6$/MeCN supporting electrolyte and about 1 mM of the analyte. All solutions were prepared under a dinitrogen atmosphere in the glovebox. Appropriate potentials were applied by using a Bioanalytical Systems (BAS) CV 50W voltammograph, and the current was carefully monitored throughout the electrolysis. By this method, the electrogenerated species (which are otherwise unstable) were obtained in situ, and their absorption spectra were recorded at regular intervals throughout the electrolysis. The attainment of a steady-state spectrum and the decay of the current to a constant minimum at a potential appropriately beyond $E_{1/2}$ (for the redox process in question) was indicative of the complete conversion of the starting material. The reversibility of the spectral data was confirmed by the regeneration of the starting spectrum.

Mass Spectrometry. Mass spectra were acquired in positive ion mode using a quadrupole time-of-flight (Q-Tof) mass spectrometer equipped with a Z-spray electrospray ionization (ESI) source (Q-Tof Premier, Waters, Milford, MA). Sample solutions were withdrawn from glass vials using a 250 μL Gastight syringe (Hamilton, Reno, NV) and immediately infused into the ESI probe at a flow rate of 5 μL/min using a syringe pump. Charged droplets of the sample solution were emitted from a stainless steel capillary (inner diameter 127 μm) with a nitrogen nebulizing gas flow of 800 L/h. The instrument parameters were as follows: capillary voltage 1.0 kV, sample cone 10 V, extraction cone 3 V, ion guide 3 V, source block temperature 80 °C, desolvation (nebulizing) gas temperature 150 °C, accelerating voltage into the argon-filled cell 2 V, first pumping stage pressure 1.2 mbar, ion transfer stage pressure 6×10^{-4} mbar, quadrupole analyzer pressure 2×10^{-5} mbar, argon-filled cell pressure 8×10^{-3} mbar, Tof analyzer pressure 9×10^{-7} mbar. No cone gas flow was used. For each sample, the sample cone and extraction cone voltages were adjusted to optimize signal for the ion(s) of interest, and the ESI capillary voltage was adjusted to maintain ion counts below the dead-time threshold (< 0.1 ions per push) to prevent spectral distortion effects because of detector saturation. The Tof analyzer was operated in "W" mode. Under these conditions, a mass resolving power, R, of 1.5×10^4 was achieved, where $R = m/\Delta m_{50\%}$, m is the mass-to-charge ratio of an ion, and $\Delta m_{50\%}$ is the full width of the mass spectral peak at half-maximum height. This was sufficient to resolve the isotopic distributions of the singly and multiply charged ions measured in this study. Thus, an ion's mass and charge could be determined independently, that is, an ion's charge state can be determined from the reciprocal of the spacing between adjacent isotope peaks in the m/z spectrum. External mass calibration was performed using solutions of sodium formate immediately prior to measuring samples. Mass spectra were processed using MassLynx software (version 4.1, Waters). In the case of **10**, reactants were mixed immediately prior to injection and the syringe was stored at −4 °C until immediately before use. In this way, we maintained the metastable forms of the analytes.

Irradiation Measurements. The optical studies were performed with a home-built reflectivity system. Operating temperatures range from 4.2 to 300 K. The spectrometric range runs from 300 to 1070 nm. The optical measurement chain is very sensitive to minimize the irradiation employed for spectrometry. This allows us to collect independently (i) the spectrometric information (by a high sensitivity Hamamatsu 10083CA spectrometer) and (ii) the photoinduced changes in the compound. The light source for spectrometric measurements was a halogen-tungsten light source (Leica CLS 150 XD tungsten halogen source adjustable from 0.5 mW/cm^2 to 1 W/cm^2 or Ocean Optic DT-MINI-2-GS deuterium tungsten halogen lamp that delivers power as low as 0.05 mW/cm^2). To induce spectrometric changes in the compound, high power irradiations (up to several mW/cm^2) have been used from a set of photodiodes (Nichia for UV, Lumileds Luxeon V for visible, Roithner for near IR). The measurements were calibrated using a NIST traceable standard for reflectance (sphereOptics, ref SG3054).

Other Physical Measurements. UV−vis−NIR diffuse reflectance and solution spectra were collected using a CARY 5000 spectrophotometer interfaced with Varian WinUV software. Infrared spectra were obtained on a Perkin-Elmer Spectrum 100 Optica FTIR spectrometer furnished with an attenuated total reflectance accessory (ATR). Elemental (C, H, and N) analyses were performed at the Microanalytical Laboratory of the University of California, Berkeley.

Results and Discussion

$PY5Me_2$ Precursor Complexes. Syntheses of the $[(PY5Me_2)M]^{2+}$ building units were carried out through a two-step reaction sequence. First, addition of solid $PY5Me_2$ to a stirred THF solution containing MX_2 (for M = Co and Ni, X = I; for M = Cu, X = Cl) led to isolation of the compounds $[(PY5Me_2)MI]I$ (M = Co (**1**), Ni (**2**)) and $[(PY5Me_2)CuCl]Cl$ (**3**). Subsequent addition of $TlPF_6$ to **1** and **2** or $AgPF_6$ to **3** in MeCN resulted in abstraction of the coordinated halide, giving the compounds $[(PY5Me_2)M(MeCN)](PF_6)_2$ (M = Co (**4**), Ni (**5**), Cu (**6**)).

X-ray crystallographic analyses of single crystals of complexes **4** and **5** revealed an octahedral coordination environment for each M^{II} center, featuring five coordination sites blocked by a $PY5Me_2$ ligand and the other bound by an MeCN ligand (see the Supporting Information, Figures S1 and S2). The mean $M-N_{py}$ bond distances (2.13(1) Å for **4** and 2.09(2) Å for **5**) are similar to those observed in complexes featuring Co^{II} and Ni^{II} centers coordinated to pyridyl ligands.[17,18] The crystal structure of **6** exhibits an asymmetric unit consisting of two distinct $[(PY5Me_2)Cu]^{2+}$ molecules (see Supporting Information, Figure S3), where both units feature a square pyramidal coordination geometry for the Cu^{II} ion. In one molecule, the coordination environment of the Cu^{II} ion consists solely of a pentacoordinate $PY5Me_2$ ligand, with the nitrogen atom of a weakly associated MeCN molecule positioned 2.514(6) Å from the open face of the basal plane. The other molecule features a Cu^{II} ion bound by a κ^4-$PY5Me_2$ ligand in a seesaw coordination, where the unbound pyridyl ring is canted away from the Cu^{II} ion. The Cu^{II} center is bound by an MeCN ligand in the remaining basal position, with a Cu−N bond distance of 2.015(6) Å, to complete the square pyramid. Variable-temperature dc magnetic susceptibility measurements performed on polycrystalline samples of **4**, **5**, and **6** gave values at 300 K of $\chi_M T = 3.17$, 1.17, and 0.39 cm^3 K/mol,

(17) (a) Wentworth, R. A. D.; Dahl, P. S.; Huffmann, C. J.; Gillum, W. O.; Streib, W. E.; Huffman, J. C. *Inorg. Chem.* **1982**, *21*, 3060. (b) Newkome, G. R.; Majestic, V. K.; Fronczek, F. R. *Inorg. Chim. Acta* **1983**, *77*, L47. (c) Xu, H.; Song, Y.; Hou, H. *Inorg. Chim. Acta* **2004**, *357*, 3541. (d) Barboiu, M.; Petit, E.; Vaughan, G. *Chem.—Eur. J.* **2004**, *10*, 2263.

(18) (a) Drew, M. G. B.; Nelson, J.; Nelson, S. M. *J. Chem. Soc., Dalton Trans.* **1981**, *8*, 1691. (b) Xu, Z.; Thompson, L. K.; Black, D. A.; Ralph, C.; Miller, D. O.; Leech, M. A.; Howard, J. A. K. *J. Chem. Soc., Dalton Trans.* **2001**, *13*, 2042. (c) Park, H. W.; Sung, S. M.; Min, K. S.; Bang, H.; Suh, M. P. *Eur. J. Inorg. Chem.* **2001**, *11*, 2857. (d) Park, K.-M.; Whang, D.; Lee, E.; Heo, J.; Kim, K. *Chem.—Eur. J.* **2002**, *8*, 498.

respectively (see Supporting Information, Figures S4−S6), confirming the expected presence of $S = {}^5/_2$, 1, and ${}^1/_2$ spin ground states with g values of 2.60, 2.16, and 2.05, respectively. In all cases, the $\chi_M T$ versus T plots show no significant temperature dependence until reaching low temperature, consistent with Curie behavior and thus magnetically isolated spin carriers. In the case of **4**, the decrease in $\chi_M T$ at low temperature is associated with spin−orbit coupling of the high-spin Co^{II} ion (see Supporting Information, Figure S4).

To probe the range of accessible oxidation states in the precursor complexes, cyclic voltammograms (CVs) were collected for $PY5Me_2$ and **4**−**6** dissolved in MeCN. Importantly, the CV obtained for uncoordinated $PY5Me_2$ shows the absence of any redox events in the potential range −2.0 to +1.8 V versus $Cp_2Fe/[Cp_2Fe]^+$, ensuring that any redox processes observed for **4**−**6** are metal-centered. Indeed, CVs obtained for **4**−**6** reveal reversible processes (see Supporting Information, Figures S7−S9). Specifically, the CV of **4** shows two reversible waves with $E_{1/2}$ = 0.168 and −1.466 V versus $Cp_2Fe/[Cp_2Fe]^+$, likely corresponding to the $Co^{II/III}$ and $Co^{I/II}$ couples, respectively. Similarly, two events are present in the CV of **5**, with $E_{1/2}$ = 1.320 and −1.610 V, assigned to the $Ni^{II/III}$ and $Ni^{I/II}$ couples. In contrast, the CV of **6** displays a single quasireversible reduction at $E_{1/2}$ = −0.302 V, likely corresponding to the $Cu^{I/II}$ redox couple.

Syntheses and Structures of the M_4Re Clusters. The pentanuclear cyano-bridged cluster compounds $[(PY5Me_2)_4M_4Re(CN)_7](PF_6)_5$ (M = Co (**7**), Ni (**8**), Cu (**10**)) and $[(PY5Me_2)_4Cu_4Re(CN)_7](PF_6)_4$ (**9**) were synthesized through the simple addition of a solution containing $[Re(CN)_7]^{3-}$ to a solution containing the appropriate precursor (**4**, **5**, or **6**). Notably, carrying out the reaction between $[Re(CN)_7]^{3-}$ and **6** at 25 °C produces a blue solution containing **9**, while performing the reaction at −42 °C gives a dark green solution containing **10**. Furthermore, within minutes upon standing at ambient temperature, the dark green solution undergoes a rapid color change to blue, associated with the spontaneous one-electron reduction of **10** to **9**. X-ray analyses on single crystals of **7**−**9** revealed the presence of a four-point star-like topology for each cluster, as depicted in Figures 1−3, respectively. In **7** and **8**, a $[Re(CN)_7]^{3-/4-}$ unit occupies the center of the star and is bridged through cyanide ligands to four pendant $[(PY5Me_2)M]^{2+/3+}$ units. The coordination environment of the $Re^{III/IV}$ ion approximates a pentagonal bipyramid and does not deviate significantly from that observed in $(Bu_4N)_3[Re(CN)_7]$[6] and $[(PY5Me_2)_4Mn_4Re(CN)_7]^{4+/5+}$.[8] In contrast, the $[Re(CN)_7]^{4-}$ unit in **9** features $C_{eq}-M-C_{eq}$ angles ranging from 70.9(2)° to 74.7(2)°, representing significant distortions from the 72° angle expected for an idealized pentagonal bipyramid (see Figure 3). Additionally, the equatorial cyanide ligands are buckled out of the idealized pentagonal plane, as evidenced by $C_{ax}-Re-C_{eq}$ angles of a single pentagonal pyramid ranging from 82.2(2)° to 98.9(2)°. The axial cyanide ligands lie close to along the 5-fold axis, with a $C_{ax}-Re-C_{ax}$ angle of 177.8(2)°.

In the structures of compounds **7**, **8**, and **9**, the coordination environments of the M^{II} ions differ considerably. In **7**, three of the cobalt ions feature a mean $Co-N_{py}$ distance of 2.13(3) Å, within the range usually observed

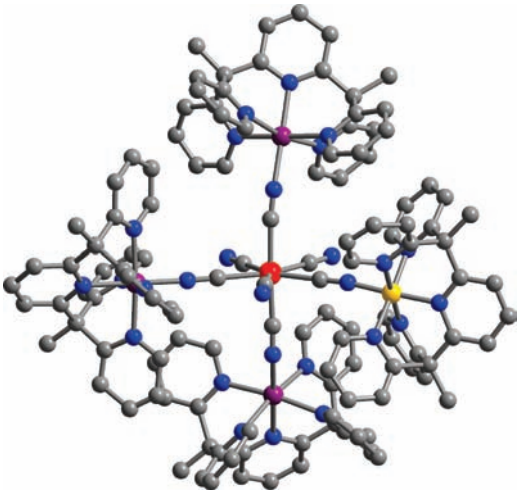

Figure 1. Structure of $[(PY5Me_2)_4Co_4Re(CN)_7]^{5+}$, as observed in **7**. Red, yellow, purple, blue, and gray spheres represent Re, Co^{III}, Co^{II}, N, and C atoms/ions, respectively; hydrogen atoms are omitted for clarity.

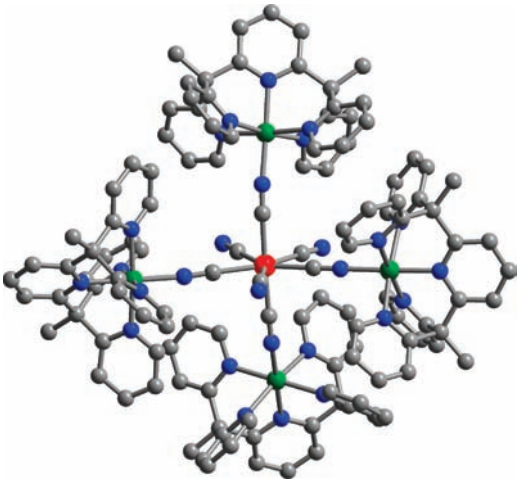

Figure 2. Structure of $[(PY5Me_2)_4Ni_4Re(CN)_7]^{5+}$, as observed in **8**. Red, green, blue, and gray spheres represent Re, Ni, N, and C atoms, respectively; hydrogen atoms are omitted for clarity.

for a Co^{II} ion bound by pyridyl ligands.[17] In stark contrast, the fourth cobalt center exhibits a significantly shorter mean distance of 1.93(4) Å. This short distance indicates the presence of a Co^{III} ion, in accordance with related pyridyl-bound Co^{III} compounds.[19] Considering charge balance in the compound, the presence of a Co^{III} ion suggests that the $[Re(CN)_7]^{3-}$ precursor has been reduced to a $[Re(CN)_7]^{4-}$ unit during the formation of **7**. In **8**, the $Ni-N_{py}$ distances clearly correspond to four octahedral Ni^{II} ions, with mean distances ranging from 2.06(5) to 2.11(6) Å. Finally, the coordination environment of each Cu^{II} ion in **9** approximates a square pyramid, with the Cu−N≡C linkage lying in the basal plane and $Cu-N_{py}$ distances not deviating significantly from those observed in **6**. The structures of **7**, **8**, and **9** all feature significantly bent M−N≡C angles, with mean angles ranging from 176.6(10)°

(19) (a) Szalda, D. J.; Keene, F. R. *Inorg. Chem.* **1986**, *25*, 2795. (b) Cabort, A.; Michel, A.; Therrien, B.; Stoeckli-Evans, H.; Bernauer, K.; Suss-Fink, G.; Williams, A. F.; Stupka, G. *Inorg. Chim. Acta* **2003**, *350*, 193. (c) Stupka, G.; Ludovic, G.; Bernardinelli, G.; Williams, A. F. *Dalton Trans.* **2004**, *3*, 407. (d) Hausmann, J.; Brooker, S. *Chem. Commun.* **2004**, *13*, 1530.

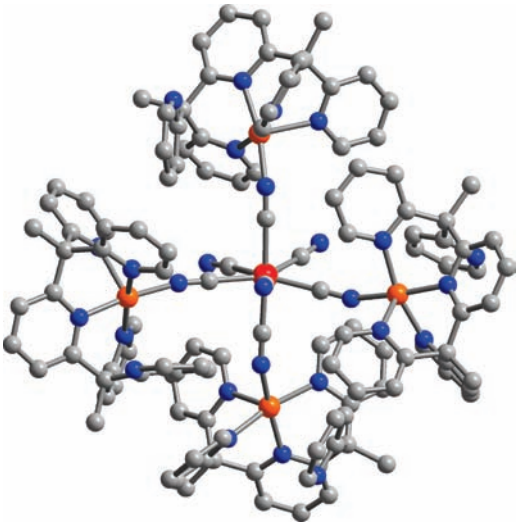

Figure 3. Structure of $[(PY5Me_2)_4Cu_4Re(CN)_7]^{4+}$, as observed in **9**. Red, orange, blue, and gray spheres represent Re, Cu, N, and C atoms, respectively; hydrogen atoms are omitted for clarity.

Table 2. Selected Mean Interatomic Distances (Å) and Angles (deg) for $[(PY5Me_2)_4M_4Re(CN)_7](PF_6)_5$ (M = Co (**7**), Ni (**8**)) and $[(PY5Me_2)_4Cu_4Re(CN)_7](PF_6)_4$ (**9**)

	7	8	9
M−N_{py}	2.13(3), 1.93(4)	2.09(2)	2.05(8)
M−NC	2.00(13)	2.03(1)	1.95(1)
M···Re	5.16(6)	5.22(4)	5.07(5)
M···M	7.6(3)	7.6(3)	7.4(2)
Re−C	2.09(2)	2.10(2)	2.10(2)
M−N≡C	165(10)	168(8)	158(8)
Re−C≡N	176(2)	177(2)	178(5)
C_{eq}−Re−C_{eq}	72(2)	72(1)	73(2)
C_{ax}−Re−C_{ax}	176(1)	175(1)	178(1)

in **7** to 152.3(4)° in **9**. Such bent angles are typical for M^{II} ions coordinated to the nitrogen end of cyanide ligands and likely arise from steric conflicts between $[(PY5Me_2)M]^{2+}$ units.[6,8,20] A summary of mean interatomic distances and angles for the structures of **7**, **8**, and **9** is given in Table 2 (see Supporting Information).

Because of the propensity for spontaneous reduction of $[Re(CN)_7]^{3-}$ upon incorporation into a cluster, all syntheses were initially performed at −42 °C. In the case of **7** and **8**, this low-temperature preparation led to products identical to those obtained from reactions conducted at ambient temperature. In the case of Cu^{II}, however, preparation at low temperature is necessary to forestall a reduction of the Re^{IV} center. Indeed, ESI mass spectrometry measurements of the chilled reaction mixture revealed the presence of an ion with a mass, charge, and isotopic distribution corresponding to that of $[(PY5Me_2)_4Cu^{II}{}_4Re^{IV}(CN)_7]^{5+}$, consistent with **10**. In contrast, a similar measurement of a solution prepared at 300 K revealed the presence of only **9** (see Supporting Information, Figure S10).

Static Magnetic Properties of the M_4Re Clusters. Variable-temperature dc susceptibility measurements were conducted to probe the magnetic exchange coupling in **7**, **8**, **9**, and **10**. A plot of $\chi_M T$ versus T for **7**, collected under an applied field of 1000 Oe, is shown in Figure 4. At 300 K, $\chi_M T$ = 7.03 cm^3 K/mol, higher than the expected value of 5.63 cm^3 K/mol for diamagnetic Re^{III} and low-spin Co^{III} ions and three isolated high-spin Co^{II} centers ($S = {}^3/_2$) with g = 2.00. This high value stems from the spin−orbit coupling of the Co^{II} ions and leads to g = 2.24. Upon lowering the temperature, $\chi_M T$ remains essentially constant to 100 K, before dropping abruptly to a minimum value of 4.56 cm^3 K/mol at 5 K. The constant value of $\chi_M T$ demonstrates the absence of any significant exchange coupling, as expected for one low-spin Co^{III} and three high-spin Co^{II} ions connected to a central diamagnetic Re^{III} center. The downturn in $\chi_M T$ below 100 K likely stems from spin−orbit coupling in the Co^{II} ions and weak antiferromagnetic coupling between Co^{II} ions through the diamagnetic Re^{III} center.[10,21] Intermolecular interactions are also possible, although unlikely in view of the separation between Co^{II} ions residing in different cluster molecules.

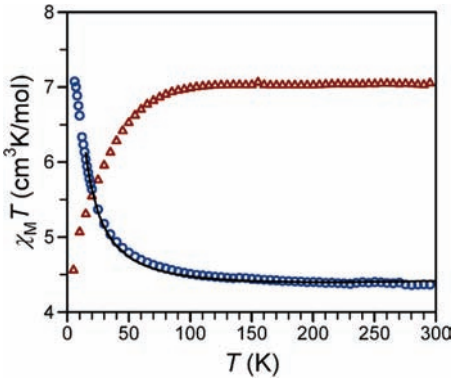

Figure 4. Variable-temperature dc magnetic susceptibility data for **7** (red triangles) and **8** (blue circles), collected under an applied field of 1000 Oe. The solid black line corresponds to a fit to the data, as described in the text, giving J = +4.4 cm^{-1}.

The temperature dependence of $\chi_M T$ observed for **8** is markedly different than that of **7**, as illustrated in Figure 4. At 300 K, $\chi_M T$ = 4.36 cm^3 K/mol, close to the expected value of $\chi_M T$ = 4.38 cm^3 K/mol for one isolated Re^{IV} center ($S = {}^1/_2$) and four isolated Ni^{II} centers (S = 1). As the temperature is decreased from 300 K, $\chi_M T$ increases monotonically to a maximum of 7.07 cm^3 K/mol at 5 K. This increase in $\chi_M T$ with decreasing temperature is indicative of ferromagnetic coupling between the Re^{IV} and Ni^{II} centers, expected for superexchange through cyanide between Re^{IV} ($e_2'^3$) and Ni ($t_{2g}{}^6e_g{}^2$) ions, giving rise to a spin ground state of $S = {}^9/_2$. The maximum at low temperature falls short of the expected value of $\chi_M T$ = 12.38 cm^3 K/mol for a spin ground state of $S = {}^9/_2$, owing in part to the strong magnetic anisotropy of the Re^{IV} center. The low magnitude of the exchange coupling constant (+4.4 cm^{-1}, as denoted below) suggests that a significant population of low lying spin excited states ($S \leq {}^7/_2$) also contributes to the unexpectedly low maximum observed in the susceptibility data.

To quantify the exchange coupling in **8**, the $\chi_M T$ data were modeled with the following isotropic spin Hamiltonian: $\hat{H} = -2J[\hat{S}_{Re}\cdot(\hat{S}_{Ni(1)} + \hat{S}_{Ni(2)} + \hat{S}_{Ni(3)} + \hat{S}_{Ni(4)})]$. In the temperature range 15−300 K, the data were fit using MAGFIT 3.1[22] to give a coupling constant of J = +4.4 cm^{-1} with

(20) (a) Naumov, N. G.; Artemkina, S. B.; Virovets, A. V.; Fedorov, V. E. *J. Solid State Chem.* **2000**, *153*, 195. (b) Mironov, Y. V.; Fedorov, V. E.; Ijjaali, I.; Ibers, J. A. *Inorg. Chem.* **2001**, *40*, 6320. (c) Brylev, K. A.; Mironov, Y. V.; Naumov, N. G.; Fedorov, V. E.; Ibers, J. A. *Inorg. Chem.* **2004**, *43*, 4833.

(21) Herrera, J. M.; Bleuzen, A.; Dromzée, Y.; Julve, M.; Lloret, F.; Verdaguer, M. *Inorg. Chem.* **2003**, *42*, 7052.

(22) Schmitt, E. A. Ph.D. Thesis, University of Illinois at Urbana-Champaign, 1995.

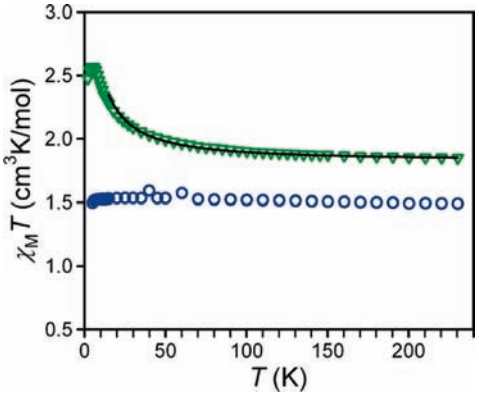

Figure 5. Variable-temperature dc magnetic susceptibility data for **9** (blue circles) and **10** (green triangles), collected under an applied field of 1000 Oe. The black line represents a fit to the data, as described in the text, giving $J = +6.26\ cm^{-1}$.

$g = 1.85$. This value represents a nearly 2-fold increase over the analogous Mn_4Re cluster, where competitive ferromagnetic and antiferromagnetic interactions lower the overall exchange strength.[8,10]

The plot of $\chi_M T$ versus T for **9**, shown in Figure 5, reveals a value of $\chi_M T = 1.48\ cm^3$ K/mol at 300 K, in agreement with the expected value of $\chi_M T = 1.50\ cm^3$ K/mol for four isolated Cu^{II} centers ($S = {}^1/_2$) and a diamagnetic Re^{III} ion. Upon lowering the temperature, $\chi_M T$ remains constant down to 5 K, as expected for negligible exchange interactions between isolated Cu^{II} centers. In stark contrast to those observed for **9**, the $\chi_M T$ data collected for **10** demonstrate a significant dependence on temperature (see Figure 5). At 300 K, $\chi_M T = 1.85\ cm^3$ K/mol, consistent with the value of $\chi_M T = 1.88\ cm^3$ K/mol expected for one isolated Re^{IV} center ($S = {}^1/_2$) and four isolated Cu^{II} centers ($S = {}^1/_2$). As the temperature is lowered, the data increase monotonically to $\chi_M T = 2.57\ cm^3$ K/mol at 6 K, before falling sharply to $\chi_M T = 2.47\ cm^3$ K/mol at 2 K. The increase in $\chi_M T$ as the temperature is lowered demonstrates the presence of ferromagnetic exchange coupling between the Re^{IV} and Cu^{II} centers, as expected for Re^{IV} ($e_2{}'^3$) and Cu^{II} ($e^4b_2{}^2b_1{}^2a_1{}^1$). The maximum at 6 K falls short of the expected $\chi_M T = 4.375\ cm^3$ K/mol for an $S = {}^5/_2$ ground state, likely because of the magnetic anisotropy of the Re^{IV} ion and the presence of low lying excited states corresponding to $S < {}^5/_2$. Nevertheless, the data were fit analogously to those obtained for **8** to give parameters of $J = +6.26\ cm^{-1}$ and $g = 2.35$. This magnitude of J surpasses that observed in **8**, presumably from the localization of the unpaired electron in the $d_{x^2-y^2}$ orbital along the direction of magnetic exchange.

To probe the magnetic anisotropy in **8** and **10**, variable-temperature magnetization data were collected under a range of applied dc fields. The resulting plots of reduced magnetization for the compounds reveal the presence of non-superimposable isofield curves (see Figure 6) as expected for molecules exhibiting significant zero-field splitting of the spin ground state. Indeed, best fits to the data obtained for **8** using ANISOFIT 2.0[23] gave axial and transverse zero-field splitting parameters of $D = 0.93\ cm^{-1}$ and $|E| \leq 0.01\ cm^{-1}$, respectively, with $g = 1.78$.

(23) Shores, M. P.; Sokol, J. J.; Long, J. R. *J. Am. Chem. Soc.* **2002**, *124*, 2279.

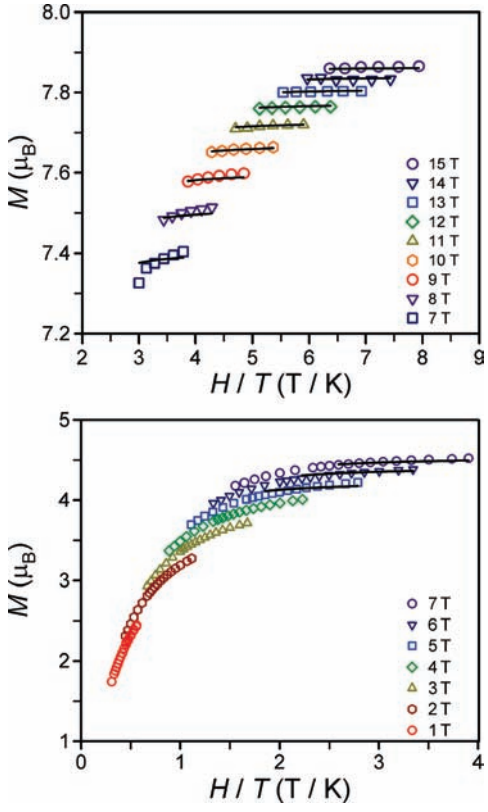

Figure 6. Low-temperature magnetization data recorded at various applied dc fields for **8** (top) and **10** (bottom). Solid black lines represent fits to the data as described in the text, giving $D = 0.93\ cm^{-1}$, $|E| \leq 0.01\ cm^{-1}$, and $g = 1.78$ for **8** and $D = -1.49\ cm^{-1}$, $|E| \leq 0.01\ cm^{-1}$, and $g = 1.95$ for **10**.

While the data were best modeled using a positive value of D, we note that determining the sign of D from magnetization data obtained for powder samples can be difficult.[10a] Indeed, ac susceptibility measurements indicate that the sign of D is in fact negative (vide infra). The best fits to the data obtained for **10** revealed parameters of $D = -1.33\ cm^{-1}$, $|E| \leq 0.01\ cm^{-1}$, and $g = 1.95$. We note that this value of D is among the largest yet reported for cyano-bridged pentanuclear single-molecule magnets[4d,k,24] and the largest recorded for a homoleptic cyanometalate-based cluster.[8] Notably, the magnitude of D is also accompanied by the lowest spin ground state of the series, as D decreases from Cu_4Re to Ni_4Re to Mn_4Re.

Dynamic Magnetic Properties of the $M^{II}_4Re^{IV}$ Clusters. To probe the relaxation dynamics in **8** and **10**, variable-temperature ac magnetic susceptibility data were collected for the two clusters under zero applied dc field at various frequencies. As shown in Figure 7, the data for **8** reveal a substantial frequency dependence of the out-of-phase (χ_M'') component of the ac susceptibility. Relaxation times (τ) were extracted from the maxima observed in χ_M'' according to the expression $\tau = 1/2\pi\nu$, where ν is the oscillation frequency of the ac field. For a single-molecule magnet, the temperature dependence of the relaxation time follows the Arrhenius relationship $\tau = \tau_0$

(24) (a) Palii, A. V.; Ostrovsky, S. M.; Klokishner, S. I.; Tsukerblat, B. S.; Berlinguette, C. P.; Dunbar, K. R. *J. Am. Chem. Soc.* **2004**, *126*, 16860. (b) Bartlett, B. M.; Harris, T. D.; DeGroot, M. W.; Long, J. R. *Z. Anorg. Allg. Chem.* **2007**, *633*, 2380.

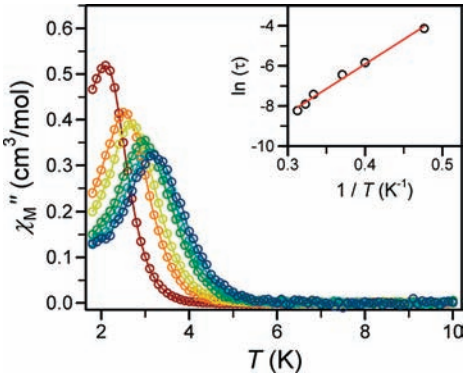

Figure 7. Variable-temperature out-of-phase ac magnetic susceptibility data for **8**, collected in a 4 Oe oscillating field at frequencies of 10 (red), 55 (orange), 100 (yellow), 267 (green), 434 (turquoise), and 601 (blue) hertz (Hz). Inset: Arrhenius plot of the relaxation time, as determined through variable-temperature ac susceptibility measurements. The solid red line corresponds to a linear fit of the data, giving $U_{eff} = 17\ cm^{-1}$.

$\exp(U_{eff}/kT)$, such that a plot of $\ln(\tau)$ versus $1/T$ should be linear, with the slope giving U_{eff}. Indeed, an Arrhenius plot constructed for **8** reveals a linear relationship, with a fit to the data affording a relaxation barrier of $U_{eff} = 17\ cm^{-1}$ with $\tau_0 = 1.4 \times 10^{-7}\ s^{-1}$. The magnitude of the energy barrier is close to the theoretical value of $U = 19\ cm^{-1}$ for an $S = {}^9/_2$ ground state with $D = -0.93\ cm^{-1}$, suggesting that quantum tunneling of the magnetization is not a major relaxation pathway in this case above 1.8 K. Additionally, the value of τ_0 gives a quantitative measure of the attempt frequency for magnetic relaxation, and the value obtained here is within the expected range for single−molecule magnets.[3,4]

Variable−temperature ac susceptibility data collected on **10** also show a frequency-dependent signal; however, this signal occurs at lower temperature such that only tails are visible in χ_M'' at temperatures down to 1.8 K (see Supporting Information, Figures S12 and S13). The spin ground state ($S = {}^5/_2$) and D value obtained from magnetization measurements give a theoretical barrier height of $8\ cm^{-1}$, consistent with the observation of only tails in the χ_M'' data.

Spectroelectrochemistry and Photomagnetic Measurements of the Co_4Re Cluster. The cyclic voltammogram of **7**, as shown in Figure 8, reveals the presence of multiple overlapping quasi−reversible peaks, the most prominent of which are situated near 0.050 and −1.8 V versus $Cp_2Fe/[Cp_2Fe]^+$. The separation between the redox processes occurring in these regions (1.85 V) is comparable to the separation of the $Co^{II/III}$ and $Co^{I/II}$ transitions in the CV of **5** (1.63 V). In view of this similarity, we hypothesize that these processes correspond to the $Co^{II/III}$ and $Co^{I/II}$ couples within the cluster, respectively. Additionally, the two quasireversible redox processes, with peak areas approximately one-third that of the other two processes, occur at $E_{1/2} = 0.762$ and 1.341 V and likely correspond to $Re^{III/IV}$ and $Re^{IV/V}$ couples, respectively.

Electronic absorption spectroscopy was employed to analyze the absorption profile of **7**. The diffuse reflectance and solution spectra collected for **7** reveal the presence of two transitions, occurring at 12,500 cm^{-1} and 20,000 cm^{-1} (see Supporting Information, Figures S14 and S15). The acetonitrile solution measurements provided molar extinction coefficients (ε) of 2,030 M^{-1} cm^{-1} and 1,930 M^{-1} cm^{-1} for the bands at 12,500 and 20,000 cm^{-1}, respectively. Additionally, bandwidths at half height ($\Delta\nu_{1/2}$) for the two absorptions are 5363 cm^{-1} and 5395 cm^{-1}, respectively. Importantly, neither of these bands is observed in the spectra of the starting materials, indicating that the observed transitions are associated with the cluster.

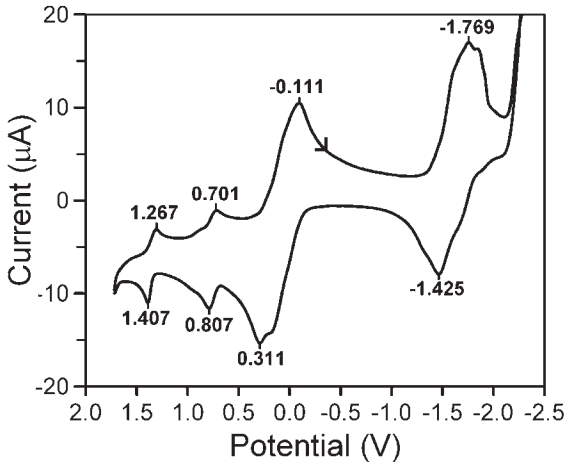

Figure 8. Electrochemical data obtained on an acetonitrile solution of **7** using a platinum electrode, 100 mV/s scan rate, and 0.1 M $(Bu_4N)PF_6$ supporting electrolyte. Potentials are reported versus $Cp_2Fe/[Cp_2Fe]^+$.

UV−Vis−NIR spectroelectrochemical measurements were performed on an acetonitrile solution containing **7**, depicted in Figure 9, to characterize the absorption bands. The spectrum changes significantly as the potential of the solution is held at +0.5 V. The lower energy band intensifies by 1000 M^{-1} cm^{-1}, while the higher energy band weakens by 700 M^{-1} cm^{-1}. Both peaks experience a concomitant blueshift of 2000 cm^{-1}. As the voltage is further increased to +1.0 V, the lower energy band at 14,000 cm^{-1} weakens in intensity by 1742 M^{-1} cm^{-1} as it shifts to a higher energy by 1650 cm^{-1}. A new transition appears at 23,000 cm^{-1} and grows to a maximum intensity of 2400 M^{-1} cm^{-1}. As the higher energy transition intensifies, it overlaps the weaker transition at 21,000 cm^{-1}, precluding a clear determination of whether the latter disappears completely during electrochemical oxidation. The lack of an isosbestic point associated with a +0.5 V applied potential is unsurprising considering the high degree of overlap observed in the CV for this potential. In contrast, an applied potential of +1.0 V is accompanied by an isosbestic point.

The presence of two bands at relatively low energy that are not observed in the spectra of the starting materials (see Supporting Information, Figures S14 and S15) suggests the occurrence of metal-to-metal charge-transfer. Indeed, the energies, intensities, and bandwidths of the two transitions are within the range expected for localized metal-to-metal charge-transfer transitions.[25] Both peaks are also highly solvatochromic. The spectroelectrochemistry experiment showed that changes to the redox states of the metal ions in the cluster caused significant changes in both the intensities and the energies of the two transitions. On the basis of these observations, we hypothesize

(25) (a) Robin, M.; Day, P. *Adv. Inorg. Chem. Radiochem.* **1967**, *10*, 247. (b) D'Alessandro, D.; Keene, F. *Chem. Soc. Rev.* **2006**, *35*, 424.

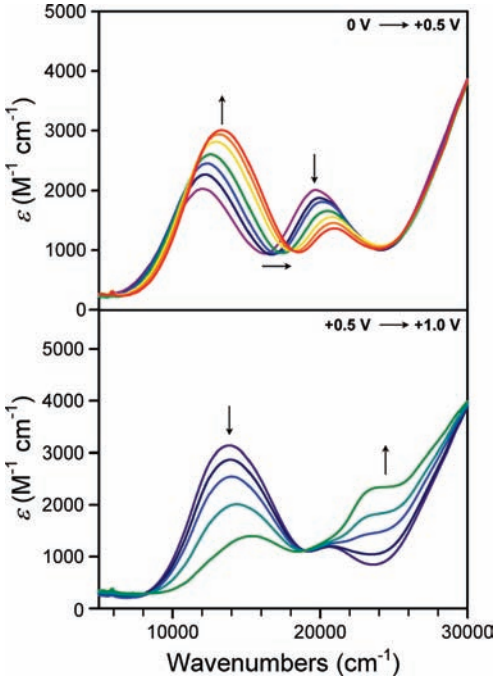

Figure 9. Spectroelectrochemical data for a 0.1 M $(Bu_4N)PF_6$ MeCN solution of **7**. The top panel displays the change in the spectrum as a +0.5 V potential is applied to the solution. The bottom graph corresponds to an applied potential of +1.0 V. Arrows indicate direction of change.

that the two low energy transitions are metal-to-metal charge-transfers (MMCTs).

While experimental evidence strongly suggests the presence of a metal-to-metal charge-transfer, assignment of the direction of the MMCT is more tentative. The reduction of Re^{IV} by one of the $[(PY5Me_2)Co]^{2+}$ units during cluster assembly suggests that perhaps one of the absorption bands could be the photon-triggered reverse process, $Re^{III}\rightarrow Co^{III}$. If the spectroelectrochemical data is analyzed under the assumption that they are Re and Co-based MMCTs, the band at 12,500 cm^{-1} likely corresponds to Re^{III} and Co^{III}, while the one at 20,000 cm^{-1} involves Re^{III} and Co^{II}. In the CV, the processes at 0.05 V were assigned to $Co^{II/III}$ couples. On the basis of this assignment, a decrease in the $Re^{III}-Co^{II}$ transitions should be observed as the Co^{II} ions within the cluster are oxidized to Co^{III}, concomitant with an increase in the intensity of the $Re^{III}-Co^{III}$ absorption. This change is indeed observed in the data. If the direction of the transfer is labeled $Re^{III}\rightarrow Co^{III}$, then a decrease in the $Re^{III}\rightarrow Co^{III}$ MMCT should be seen as a +1.0 V potential is applied. In addition, the 0.762 V process was assigned to the $Re^{III/IV}$ couple. If that assignment is correct, then as Re^{IV} is produced a decrease in the $Re^{III}\rightarrow Co^{III}$ MMCT should occur, since Re^{IV} would have less electron density to transfer to the pendant Co^{III} ions. Furthermore, since Re^{IV} has a singly-occupied metal-centered orbital, the appearance of a relatively higher energy ligand-to-metal charge transfer (LMCT) would be expected. Indeed, this is observed with the emergence of the absorption at 23,000 cm^{-1}, although the assignment of this band as a LMCT is purely based on the above assumptions. The presence of an isosbestic point gives credence to the assignment of the 0.762 V process as $Re^{III/IV}$ because there is only one Re per cluster molecule.

Our interest in the photophysical properties of **7** is spurred by the photomagnetic properties of several cyano-bridged extended framework and coordination cluster systems.[26,27] If the $Re^{III}\rightarrow Co^{III}$ MMCT state could be trapped via irradiation at low temperature, then the hypothesized $Co^{II}{}_4Re^{IV}$ state could be analyzed to probe for possible slow magnetic relaxation. The magnetic anisotropy associated with both Co^{II} and Re^{IV} ions, in conjunction with the expected $S = {}^{11}/_{2}$ spin ground state of the $Co^{II}{}_4Re^{IV}$ cluster, could give rise to a large spin-reversal barrier. Toward this end, solid-state reflectivity data were collected between 290 and 10 K (under white light irradiation of 0.05 mW/cm^2). With cooling, the spectra of **7** show an increase in the absolute reflectivity in the 10,000−25,000 cm^{-1} range (see Supporting Information, Figure S16). The compound is more reflecting (or less absorbing) at low temperature, with this effect being more important in the NIR (Near Infra-Red, 13,333−25,000 cm^{-1}) region. Upon heating, the absolute reflectivity decreases, and the compound recovers at 280 K the same spectrum observed before the thermal cycle. Photoexcitation properties of **7** were studied by cooling the sample to 5 K (under a very weak white light irradiation 0.05 mW/cm^2) followed by white light irradiation (6 mW/cm^2). Rapidly, a decrease in absolute reflectivity is observed above 12,500 cm^{-1}, and after 12 min the spectrum remains unchanged (see Supporting Information, Figure S17). Upon heating, the photogenerated state decays smoothly, and the original spectrum is restored at room temperature, as observed in the thermal

(26) (a) Macknight, F.; Haight, G. P. *Inorg. Chem.* **1973**, *12*, 3007. (b) Sato, O.; Iyoda, T.; Fujishima, A.; Hashimoto, K. *Science* **1996**, *272*, 704. (c) Verdaguer, M. *Science* **1996**, *272*, 698. (d) Sato, O.; Einage, Y.; Iyoda, T.; Fujishima, A.; Hashimoto, K. *J. Electrochem. Soc.* **1997**, *144*, 11. (e) Shimamoto, N.; Ohkoshi, S.-i.; Sato, O.; Hashimoto, K. *Inorg. Chem.* **2002**, *41*, 678. (f) Bleuzen, A.; Lomenech, C.; Escax, V.; Villain, F.; Varret, F.; Cartier dit Moulin, C.; Verdaguer, M. *J. Am. Chem. Soc.* **2000**, *122*, 6648. (g) Cartier dit Moulin, C.; Villain, F.; Bleuzen, A.; Arrio, M.-A.; Sainctavit, P.; Lomenech, C.; Excax, V.; Baudelet, F.; Dartyge, E.; Gallet, J. J.; Verdaguer, M. *J. Am. Chem. Soc.* **2000**, *122*, 6653. (h) Escax, V.; Bleuzen, A.; Cartier dit Moulin, C.; Villain, F.; Goujon, A.; Varret, F.; Verdaguer, M. *J. Am. Chem. Soc.* **2001**, *123*, 12536. (i) Ohkoshi, S.; Machida, N.; Zhong, Z. J.; Hashimoto, K. *Synth. Met.* **2001**, *122*, 523. (j) Rombaut, G.; Verelst, M.; Golhen, S.; Ouahab, L.; Mathonière, C.; Kahn, O. *Inorg. Chem.* **2001**, *40*, 1151. (k) Ohkoshi, S.-i.; Machida, N.; Abe, Y.; Zhong, Z. J.; Hashimoto, K. *Chem. Lett.* **2001**, 312. (l) Shimamoto, N.; Ohkoshi, S.; Sato, O.; Hashimoto, K. *Chem. Lett.* **2002**, *31*, 486. (m) Liu, H. W.; Matsuda, K.; Gu, Z. Z.; Takahashi, K.; Cui, A. L.; Nakajima, R.; Fujishima, A.; Sato, O. *Phys. Rev. Lett.* **2003**, *90*, 167403. (n) Gawali-Salunke, S.; Varret, F.; Maurin, I.; Enachescu, C.; Malarova, M.; Boukheddaden, K.; Codjovi, E.; Tokoro, H.; Ohkoshi, S.; Hashimoto, K. *J. Phys. Chem. B* **2005**, *109*, 8251. (o) Varret, F.; Boukheddaden, K.; Codjovi, E.; Maurin, I.; Tokoro, H.; Ohkoshi, S.-i.; Hashimoto, K. *Polyhedron* **2005**, *24*, 2857. (p) Ohkoshi, S.-i.; Ikeda, S.; Hozumi, T.; Kashiwagi, T.; Hashimoto, K. *J. Am. Chem. Soc.* **2006**, *128*, 5320. (q) Tokoro, H.; Matsuda, T.; Nuida, T.; Morimoto, Y.; Ohoyama, K.; Loutete−Dangui, E. D.; Boukheddaden, K.; Ohkoshi, S.-i. *Chem. Mater.* **2008**, *20*, 423. (r) Bleuzen, A.; Marvaud, V.; Mathonière, C.; Sieklucka, B.; Verdaguer, M. *Inorg. Chem.* **2009**, *48*, 3453.

(27) (a) Marvaud, V.; Decroix, C.; Scuiller, A.; Tuyéras, F.; Guyard-Duhayon, C.; Vaissermann, J.; Marrot, J.; Gonnet, F.; Verdaguer, M. *Chem.—Eur. J.* **2003**, *9*, 1692. (b) Herrera, J.-M.; Marvaud, V.; Verdaguer, M.; Marrot, J.; Kalisz, M.; Mathonière, C. *Angew. Chem., Int. Ed.* **2004**, *43*, 5468. (c) Dei, A. *Angew. Chem., Int. Ed.* **2005**, *117*, 1184. (d) Mathonière, C.; Podgajny, R.; Guionneau, P.; Labrugère, C.; Sieklucka, B. *Chem. Mater.* **2005**, *17*, 442. (e) Sato, O.; Tao, J.; Zhang, Y.-Z. *Angew. Chem., Int. Ed.* **2007**, *46*, 2152. (f) Li, D.; Clérac, R.; Roubeau, O.; Harte, E.; Mathonière, C.; Le Bris, R.; Holmes, S. M. *J. Am. Chem. Soc.* **2008**, *130*, 252. (g) Tuyéras, F.; Scuiller, A.; Duhayon, C.; Hernandez-Molina, M.; Fabrizi de Biani, F.; Verdaguer, M.; Mallah, T.; Wernsdorfer, W.; Marvaud, V. *Inorg. Chim. Acta* **2008**, *361*, 3505. (h) Mathonière, C.; Kobayashi, H.; Le Bris, R.; Kaiba, A.; Bord, I. C. *Chimie* **2008**, *11*, 665.

variation of $R_{10,000cm^{-1}}$ (see Supporting Information, Figure S18). A similar behavior is obtained when the compound is irradiated at 5 K with a blue light of 21,277 cm^{-1} (6 mW/cm^2). This optical reflectivity study shows that **7** is thermochromic and photochromic using white and blue irradiation lights.

Magnetic measurements of an irradiated sample of **7** were performed at low temperatures with a variety of light sources. Although the reflectivity measurements suggest population of an excited state, a small photomagnetic effect at 10 K is observed as a decrease in $\chi_M T$ of about 1% when the compound is irradiated with blue light (21,277 cm^{-1}, 6 mW/cm^2). In line with the rapid saturation of the photoactivity observed in the reflectivity measurements, the very dark color of the crystals suggests that light cannot easily penetrate the material, thus highlighting the possibility that the photogenerated state is occurring mainly on the surface of the material.

Outlook

The foregoing results demonstrate the utility of the building unit $[Re(CN)_7]^{3-}$ in the preparation of new star-like clusters of formulas $[(PY5Me_2)_4M_4Re(CN)_7]^{n+}$ (M = Co, Ni, Cu). The formation of the Co_4Re cluster is accompanied by a one-electron transfer from cobalt to rhenium. In contrast, use of the electron-rich precursor complex $[(PY5Me_2)Ni]^{2+}$ in the cluster assembly forestalls a spontaneous reduction of the Re^{IV} ion and thus enables access to a redox-stable Ni_4Re cluster, which demonstrates slow magnetic relaxation at low temperature. Future efforts will focus on extending this synthetic strategy to star-like clusters bearing second- and third-row transition metals as the pendant metal centers, thereby providing a route to stronger magnetic anisotropy. In a parallel strategy, clusters featuring electron-rich $[(PY5Me_2)M]^{2+}$ units with unquenched orbital angular momentum will be targeted. It is our hope that such efforts to strengthen the magnetic anisotropy and increase the redox stability of high-nuclearity clusters incorporating $[Re(CN)_7]^{3-}$ will lead to the discovery of new single-molecule magnets with considerably larger relaxation barriers.

Acknowledgment. This work was supported by NSF Grant CHE-0617063 and the France-Berkeley Fund the University of Bordeaux, the CNRS, the ANR (NT09_469563, AC-MAGnets project), the Region Aquitaine and the GIS Advanced Materials in Aquitaine (COMET Project). We thank Tyco Electronics for providing D.E.F. and T.D.H. with predoctoral fellowships. We thank Dr. F. J. Hollander, Dr. A. DiPasquale, Dr. J. O'Brien, and Dr. D. M. D'Alessandro for insightful discussions and experimental assistance.

Supporting Information Available: Crystallographic information files, full crystal tables for **4**−**9**, and plots showing additional data. This material is available free of charge via the Internet at http://pubs.acs.org.